

## Si/Ag NANOCOMPOSITE LITHIUM-ION BATTERY ANODE WITH ENHANCED PERFORMANCE USING (3-MERCAPTOPROPYL) TRIMETHOXYL SILANE AS CROSS-LINKER

S. XIE<sup>a</sup>, Q. JI<sup>a,b</sup>, Y. XIA<sup>a</sup>, S. YIN<sup>a,c</sup>, K. FANG<sup>a,d</sup>, M. WANG<sup>a</sup>, X. WANG<sup>a</sup>, J. BAN<sup>a,d</sup>, Y. ZHANG<sup>a,c</sup>, B. QIU<sup>a</sup>, Z. LIU<sup>a</sup>, J. ZHU<sup>a</sup>, Y. J. CHENG<sup>a,e\*</sup>

<sup>a</sup>Ningbo Institute of Materials Technology & Engineering, Chinese Academy of Sciences, 1219 Zhongguan West Rd, Ningbo, 315201, Zhejiang Province, P. R. China

<sup>b</sup>The University of Nottingham Ningbo China, 199 Taikang East Road, Ningbo, 315100, Zhejiang Province, P. R. China

<sup>c</sup>North University of China, Shanglan Rd, Taiyuan, 030051, Shanxi Province, P. R. China

<sup>d</sup>Nano Science and Technology Institute, University of Science and Technology of China, 166 Renai Rd, Suzhou, 215123, Jiangsu Province, P. R. China

<sup>e</sup>Department of Materials, University of Oxford, Parks Rd, OX1 3PH, Oxford, UK

A new concept is developed to significantly improve the cyclic stability and rate performance of the silicon based lithium-ion battery anode with high mass loading density. (3-Mercaptopropyl) trimethoxyl silane (MPTMS) is used as a cross-linking agent to bind the silicon and silver nanoparticles together by forming coordination and covalent bonding on the surface of the nanoparticles, as confirmed by the FTIR measurement. It is found that with MPTMS the reversible capacity can be effectively lifted to 517 mAh/g compared to the bare Si/Ag (near zero) after 100 cycles at 200 mA/g. Better rate performance is also achieved with the incorporation of the MPTMS. The morphologies of the electrodes before and after cycling show that the Si/Ag nanocomposites modified with MPTMS exhibit better structure integrity.

(Received November 25, 2016; Accepted February 24, 2017)

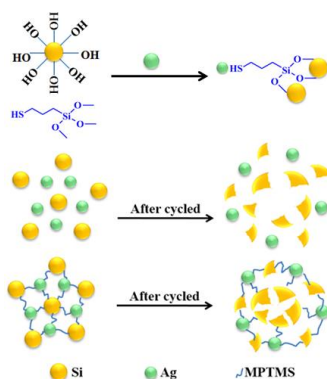
*Keywords:* nanocomposite, battery, electrodes, Si/Ag

### 1. Introduction

Silicon has been regarded as one of the most promising next generation lithium-ion battery anode<sup>1-5</sup>. It is featured with ultrahigh theoretical specific capacity (4200 mAh/g) compared to the commercial graphite (372 mAh/g). The proper charge-discharge potential of 0.2 V - 0.4 V (vs. Li/Li<sup>+</sup>) makes a good balance between avoiding excessive lithium plating and providing high voltage output. However, several severe drawbacks limit the practical applicability of the Si anode. Firstly, the drastic volume change (*ca.* 400 %) of silicon upon lithiation and delithiation causes very poor cyclic stability. Secondly, Silicon has low electron conductivity as a semiconductor, which provides limited rate performance<sup>6-14</sup>. Tremendous efforts have been made to solve these problems including reducing particle size to nanometer scale<sup>15-20</sup>, compositing with conductive and/or buffer medium, and constructing hierarchical structure<sup>21-28</sup>. Among the different buffer medium, metals such as silver nanoparticles have particular advantages. Firstly, the silver nanoparticles possess excellent ductile ability and superior mechanical strength. It can effectively absorb the mechanical stress generated by the volume change of silicon. Secondly, the silver nanoparticles inherit outstanding electron conductivity, which can enhance the electrochemical kinetics during lithiation/delithiation. Much work has been reported about the synthesis of Si/Ag nanocomposites to improve the performance of the silicon based lithium-ion battery anode<sup>29-34</sup>. However, little attention has been paid to the surface engineering of both silicon and silver species.

\*Corresponding author: chengyj@nimte.ac.cn

Normally, the interaction between silicon and silver is very weak. As a result, along with repeated lithiation/delithiation process, the silicon and silver nanoparticles tend to lose contact (**Scheme 1**). On one hand, the silver nanoparticles cannot absorb the mechanical stress induced by volume change in an efficient way. The crack of the silicon particles and pulverization of the electrode cannot be effectively suppressed. On the other hand, the charge carrier transportation are inhibited, leading to poor kinetics of the lithiation/delithiation process. Overall, the cyclic stability and rate performance of the Si anode are significantly deteriorated with increasing cycles. Here in this work, a new concept has been introduced to enhance the interaction between silicon and silver nanoparticles for the first time (Scheme 1). (3-Mercaptopropyl) trimethoxyl silane (MPTMS) is employed as a cross-linker to connect both silicon and silver nanoparticles through strong covalent and coordination bonding at molecular level. The Si/Ag/MPTMS nanocomposites are prepared in a facile way by adding the (3-Mercaptopropyl) trimethoxyl silane to the Si/Ag suspension through ultrasonication. The MPTMS bears difunctional groups on each side of the molecule. While the thiol functional group on one end has a high affinity to bind the silver nanoparticles, the silane group on the other end reacts with the hydroxyl group on the silicon surface to form Si-O-Si bond effectively<sup>35-37</sup>. With the cross-linking agent of MPTMS, both the silicon and silver nanoparticles are bound together. Even the silicon nanoparticles are cracked with repeated drastic volume change, partial local contact between silicon and silver tends to be retained, leading to improved performance (Scheme 1).



*Scheme 1. Schematic feature of the cross-linking between silicon and silver nanoparticles by MPTMS (a), structure change of the Si/Ag (b), and Si/Ag/MPTMS (c) nanocomposites before and after cycling.*

## 2. Experiment

### 2.1. Sample Preparation

All reagents were used as received without further purification. Silicon nanoparticles (30 nm, 99.9 % in purity) were purchased from HT-NANO Shanghai, China. Silver nanoparticles (80 nm – 90 nm, 99.9 % in purity) were bought from XFNANO Materials Tech Co., Ltd, Nanjing, China. (3-Mercaptopropyl) trimethoxyl silane was obtained from Aladdin. Absolute ethanol was purchased from Sinopharm. Sodium alginate was purchased from Aladdin Reagent Co., Ltd., China. Conductive carbon Super P was bought from SCM Chem. Shanghai, China.

0.2 g silicon nanoparticles were dispersed in 5 mL anhydrous ethanol by ultrasonication for 30 min. Then certain amounts of (3-Mercaptopropyl) trimethoxyl silane (abbreviated as MPTMS) were added into the Si/ethanol dispersion, followed by addition of 0.1 g Ag nanoparticles. The suspension was further ultrasonicated for an hour to achieve homogeneous dispersion of the Si and Ag nanoparticles in ethanol and allow cross-linking reaction between MPTMS and Si/Ag nanoparticles. Thereafter, centrifugation (8000 rpm, 3 times, 10 min each time) was applied to remove the non-reacted MPTMS and collect the Si/Ag/MPTMS nanocomposites, followed by washing with anhydrous ethanol for three times and drying in vacuum over at 80 °C overnight. The Si/Ag nanoparticles modified with the MPTMS amounts of 0 g, 0.2 g, 0.6 g, and 0.8 g were indexed as M-0, M-0.2, M-0.6, and M-0.8 respectively.

## 2.2. Sample Characterization

Scanning electron microscope (SEM) images were obtained with Hitachi S4800 scanning electron microscope at an accelerating voltage of 4 kV. The samples were put on a conductive tape and sputtered with gold before imaging. X-ray diffraction (XRD) patterns were recorded with Bruker D8 diffractometer with  $2\theta$  ranging from  $5^\circ$  to  $90^\circ$  (Cu  $K\alpha$ ,  $\lambda = 0.15406$  nm). FTIR analysis was carried out by NICOLET 6700 Fourier transform infrared spectroscopy with an average 64 scans.

## 2.3. Coin Cell Assembly and Electrochemical Testing

2032-type coin cells composed of a cylindrical pad with 20 mm in diameter and 3.2 mm in height were fabricated using lithium foil as a counter electrode. The slurry mixture was prepared by mixing the active materials, conductive acetylene black carbon (super P), and sodium alginate in deionized water with a mass ratio of 8:1:1 through manual grinding in mortar. The electrodes were fabricated by spreading the slurry on copper foil with doctor blading, followed by drying at  $80^\circ\text{C}$  in oven for 4 h. After drying, the cast copper foil was pressed and cut into round shaped electrode with a diameter of 13 mm. The loading mass on the electrode was weighed using a balance with the resolution of 0.01 mg. Before cell assembly, the electrode was further dried in oven at  $80^\circ\text{C}$  for several hours. The Celgard 2400 microporous polypropylene membrane was used as separator. Electrolyte (Dongguan shanshan battery material Co., Ltd) was used where 1.0 M  $\text{LiPF}_6$  was dissolved in a mixture of ethylene carbonate (EC) and dimethyl carbonate (DMC) (1:2 v/v). The mass loading density was controlled to be in the range between  $1.1\text{ mg/cm}^2$  and  $1.2\text{ mg/cm}^2$  based on the total mass of the Si/Ag/MPTMS nanocomposite. The cyclic and rate performance of the coin cells were tested using a multichannel Land Battery Test System. The cyclic performance was measured at a current density of 0.2 C (1 C = 1000 mAh/g) for 100 cycles in the voltage range of 3.0 V - 0.005 V (vs.  $\text{Li/Li}^+$ ). The specific capacity was calculated on the basis of the active materials, which was the total mass of the silicon, silver, and MPTMS. The rate performance measurement was carried out at the current density sequence of 0.1 C, 0.2 C, 0.5 C, and 1 C (each current density for 5 cycles) in the voltage range between 3.0 V and 0.005 V (vs.  $\text{Li/Li}^+$ ). The lithiation process was defined as the discharge process, while the de-lithiation process was referred as the charging process. The cyclic voltammetry tests were measured by CHI 1040B potentiostat/galvanostat analyzer (Shanghai Chenhua instrument Co., Ltd.) at a scanning rate of 0.01 mV/s with the voltage range between 0.001 V and 3.0 V. The electrochemical impedance spectroscopy (EIS) measurement was conducted on an Autolab modular electrochemical system (Autolab PGSTAT302N) over a frequency range from 100 KHz to 0.01 Hz.

## 3. Results and discussion

Fig. 1 shows the XRD patterns of the Si/Ag/MPTMS series of samples. All of the nanocomposites added with different amounts of MPTMS exhibit identical diffraction peaks, corresponding to the crystalline phases of silicon and silver. Specifically, the two-theta peaks located at  $28^\circ$ ,  $47^\circ$ ,  $56^\circ$ ,  $69^\circ$ ,  $76^\circ$ , and  $88^\circ$  are assigned to the face-centered cubic phase of silicon (JCPDS No.27-1402). The peaks at  $38^\circ$ ,  $44^\circ$ ,  $64^\circ$ ,  $77^\circ$ ,  $76^\circ$ , and  $82^\circ$  correspond to the cubic phase of silver (JCPDS No. 04-0783). The XRD results indicate that the surface functionalization with different amounts of MPTMS does not modify the crystallinity of both silicon and silver. Furthermore, besides the peaks belonging to silicon and silver, no additional diffraction peaks are observed. It suggests that there is no detectable amount of crystalline MPTMS formed within the Si/Ag nanocomposite powders.

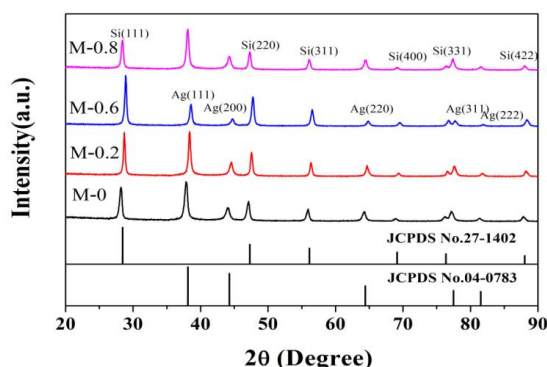


Fig. 1. XRD patterns of the Si/Ag/MPTMS (Si: 0.2 g, Ag: 0.1 g) nanocomposites cross-linked with different amounts of MPTMS: 0 g (M-0), 0.2 g (M-0.2), 0.6 g (M-0.6), and 0.8g (M-0.8).

Fig. 2 is the FTIR spectra of the Si/Ag nanocomposites modified with different amounts of MPTMS. The FTIR spectrum proves that MPTMS is successfully incorporated into the Si/Ag nanocomposites. Compared to the bare Si/Ag sample, new peaks appear in the region between  $600\text{ cm}^{-1}$  and  $800\text{ cm}^{-1}$  with respect to the Si/Ag/MPTMS nanocomposites. The peaks at  $649\text{ cm}^{-1}$  and  $742\text{ cm}^{-1}$  are ascribed to the stretch vibration of the C-S bond. And the peak of  $1100\text{ cm}^{-1}$  is ascribed to the stretch vibration of the SiO-C bond. Finally, the peaks between  $1140\text{ cm}^{-1}$  and  $1250\text{ cm}^{-1}$  originate from the stretch vibration of the C-C bond of the alky chains<sup>38-39</sup>.

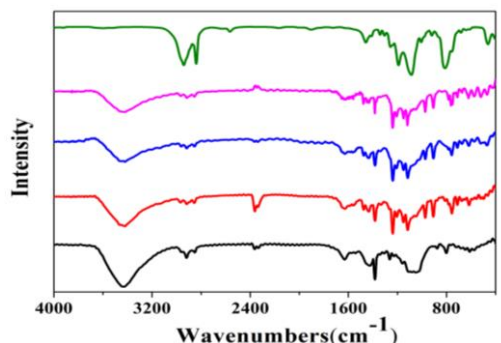


Fig. 2. FTIR spectra of the Si/Ag/MPTMS nanocomposites (Si: 0.2 g, Ag: 0.1 g) modified with different amounts of MPTMS. M-0: 0 g, M-0.2: 0.2 g, M-0.6: 0.6 g, and M-0.8: 0.8 g of MPTMS.

Fig. 3 depicts the discharge/charge profiles for the first, second, tenth, and one hundredth cycle of the Si/Ag/MPTMS nanocomposites modified with increasing amount of MPTMS. The voltage window is set between 0.005 V and 3.0 V and the current density is of 200 mA/g. All of the samples exhibit similar discharge/charge patterns. For the first cycle, there is a short slope plateau at a voltage of 1.2 V, which is due to the formation of solid electrolyte interface (SEI) film. The long flat plateaus at around 0.1 V/0.4 V are characteristic profiles for the lithiation/delithiation process of crystalline Si. No additional plateau is observed, which indicates that the silver nanoparticles are unlikely involved in the lithiation process. The M-0 sample delivered an initial discharge specific capacity of 2255 mAh/g and a reversible capacity of 1976 mAh/g, corresponding to an initial coulombic efficiency of 88 %. With increasing amount of MPTMS, the initial discharge/charge capacities and coulombic efficiencies of the Si/Ag nanocomposites do not change significantly. It indicates that the binding of MPTMS to silicon and silver nanoparticles

does not modify the initial discharge/charge behavior. The discharge/charge profiles of the subsequent cycles are similar which indicates a stable electrochemical process of the nanocomposite electrodes. Particularly, the specific capacity of the M-0 sample drops to nearly zero when cycled to the 100<sup>th</sup> cycle. However, the specific capacities of the Si/Ag nanocomposites modified with MPTMS still reach several hundred mAh/g. The representative discharge/charge profiles imply that the addition of MPTMS significantly improves the discharge/charge capacities of the Si/Ag nanocomposites over 100 cycles.

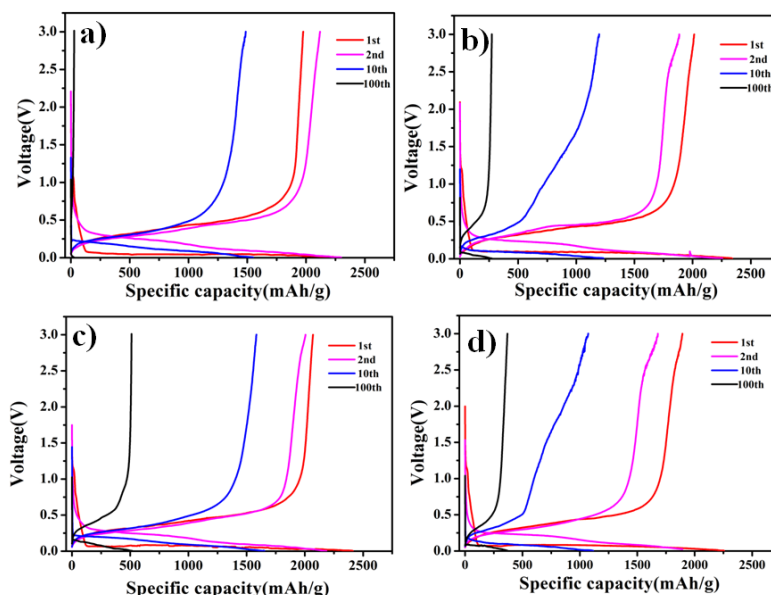


Fig. 3. Voltage profiles of the Si/Ag nanocomposite electrodes modified with different amounts of MPTMS (Si: 0.2 g, Ag: 0.1 g), cycled between 0.005 V and 3 V at 200 mA/g.

M-0 (0 g, a), M-0.2 (0.2 g, b), M-0.6 (0.6 g, c), and M-0.8 (0.8 g, d).

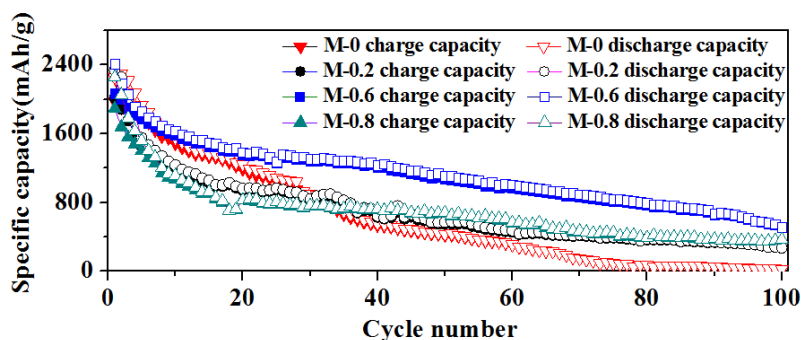


Fig. 4. Cyclic performance of the Si/Ag nanocomposite electrodes modified with different amounts of MPTMS (Si: 0.2 g, Ag: 0.1 g) at current density of 200 mA/g. M-0 (0 g), M-0.2 (0.2 g), M-0.6 (0.6 g), and M-0.8 (0.8 g).

The detailed cyclic performance of the Si/Ag/MPTMS nanocomposites at the current density of 200 mA/g is further shown in Fig. 4. The Si/Ag nanocomposites modified with increasing amounts of MPTMS exhibit better cyclic performance than the bare Si/Ag nanocomposite. Particularly, the reversible capacity of the M-0.6 sample after 100 cycles reaches more than 500 mAh/g. It should be pointed out that the mass loading density of the electrodes are quite higher (more than 1 mg/cm<sup>2</sup>) than typically values reported previously. As a result, the absolute reversible capacity values are sacrificed because of the high mass loading density. However, practically relevant data are provided, which is meaningful for real application of the silicon based anode. While the capacity of the bare Si/Ag nanocomposite (M-0) drops to nearly

zero. The MPTMS acts as a cross-linker between Si and Ag nanoparticles by forming Ag-S coordination bond and Si-O-Si covalent bond simultaneously. It causes multiple impacts on the electrochemical performance of the Si/Ag nanocomposite electrode. First, the overall mechanical properties of the Si/Ag electrode is improved, which helps to inhibit the pulverization process of the electrode induced by drastic volume change of the silicon nanoparticles. Second, the MPTMS cross-linking agent enhances the local contact between neighboring silicon and silver nanoparticles. As a result, the electronic conductive path can still be retained along with serious pulverization process. As a result, the addition of MPTMS cross-linking agent improves the structural integrity and electrochemical cyclic stability of the Si/Ag nanocomposite electrodes.

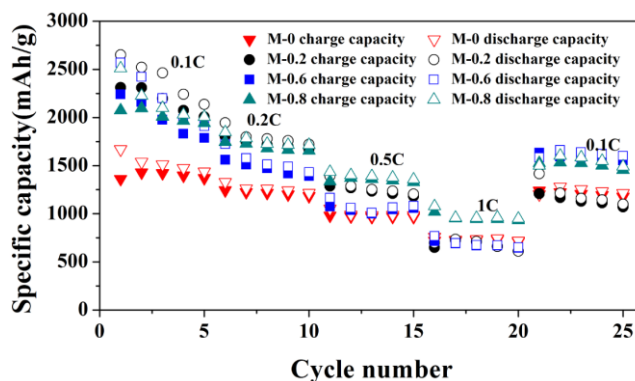


Fig. 5. Rate performance of the Si/Ag nanocomposite electrodes modified with different amounts of MPTMS (Si: 0.2 g, Ag: 0.1 g): M-0 (0 g), M-0.2 (0.2 g), M-0.6 (0.6 g), and M-0.8 (0.8 g).

Fig. 5 shows the rate performance of the Si/Ag nanocomposites modified with different amounts of MPTMS at the current density sequence of 0.1 C, 0.2 C, 0.5 C, 1 C, and 0.1 C (1 C = 1000 mA/g). Generally, the Si/Ag nanocomposites modified with MPTMS exhibit higher capacities at different current densities. The M-0.8 sample even shows a capacity of 1078 mAh/g at 1000 mA/g, which is much higher than the bare Si/Ag nanocomposite (759 mAh/g). When the current density is returned to 100 mA/g, the M-0.8 electrode shows a capacity of 1500 mAh/g compared to the capacity of the unmodified Si/Ag sample (1200 mAh/g). The results indicate that the MPTMS functionalization on the Si/Ag nanoparticles exhibit better rate performance and cyclic stability as well. The MPTMS acts as cross-linking agent to bind both silicon and silver nanoparticles together. As a result, the local contact between neighboring silicon and silver nanoparticles is improved, leading to enhanced charge carrier transportation of the nanocomposites and better rate performance at different current densities.

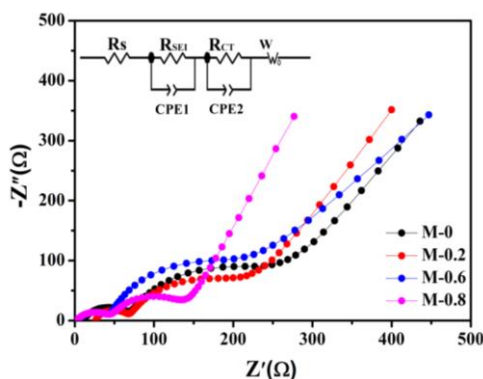


Fig. 6. Nyquist plots of the Si/Ag nanocomposite electrodes modified with different amounts of MPTMS (Si: 0.2 g, Ag: 0.1 g): M-0 (0 g), M-0.2 (0.2 g), M-0.6 (0.6 g), and M-0.8 (0.8 g).

Table 1. Major EIS fitting parameters based on equivalent model circuit.

Sample	$R_{ct}(\Omega)$	$R_{total}(\Omega)$
M-0	170	240
M-0.2	140	208
M-0.6	125	167
M-0.8	76	120

The electrochemical impedance spectroscopy (EIS) tests were performed with the coin cells cycled at 200 mA/g for three cycles. Fig. 6 shows the Nyquist plots of the Si/Ag nanocomposites modified with different amounts of MPTMS. The experimental data is fitted based on an equivalent model circuit, which is typically composed of resistances originated from ohmic contact ( $R_s$ ), SEI layer ( $R_{SEI}$ ), charge transfer process ( $R_{CT}$ ), and Warburg impedance ( $W$ ), and constant phase elements of the capacitor components. Specifically, the semicircle in the high-frequency region corresponds to the Li-ion transportation resistance. And the semicircle in the middle-frequency region represents the charge transfer resistance ( $R_{CT}$ ). And the inclined line in the low-frequency range could be assigned to the Warburg impedance<sup>40-42</sup>. The fitting results shown in Table 1 indicate that the charge transfer resistance and total resistance of the electrodes are decreased with increasing MPTMS content. It confirms that the MPTMS cross-linker bridges the silicon nanoparticles and the conductive silver nanoparticles, leading to improved electron conductivity of the nanocomposites.

The cyclic voltammetry profiles of the Si/Ag/MPTMS nanocomposites for the initial five cycles are measured with the voltage range of 0.001 V – 3 V as shown in Fig. 7. The broad weak peak at around 1.25V is due to the formation of SEI (solid electrolyte interface) layer, which only appears in the cathodic process of the first cycle<sup>41</sup>. The results are consistent with the discharge/charge profiles, where a short slope at 1.2 V is observed. A new peak at 0.2 V appears from the second cycle, which is attributed to the alloying process between lithium and silicon to form amorphous  $Li_xSi$ .

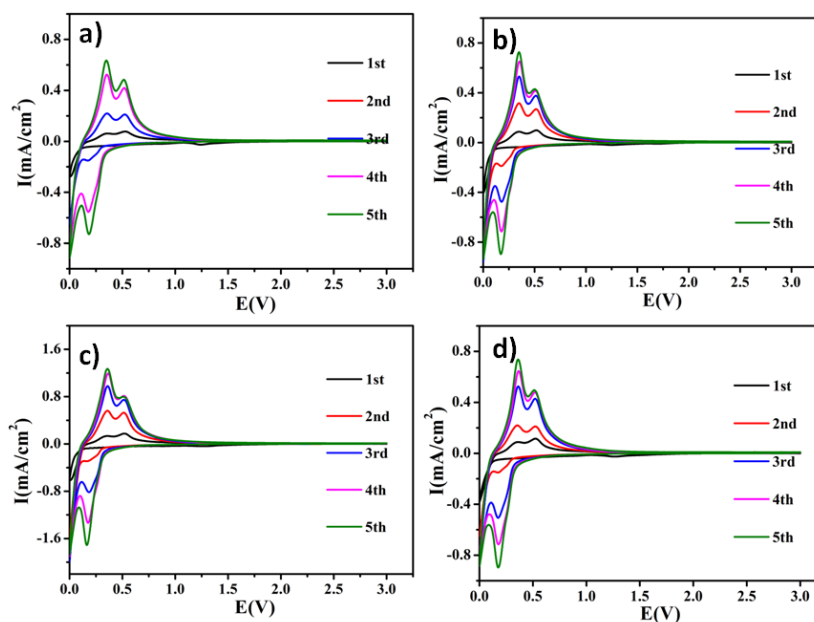
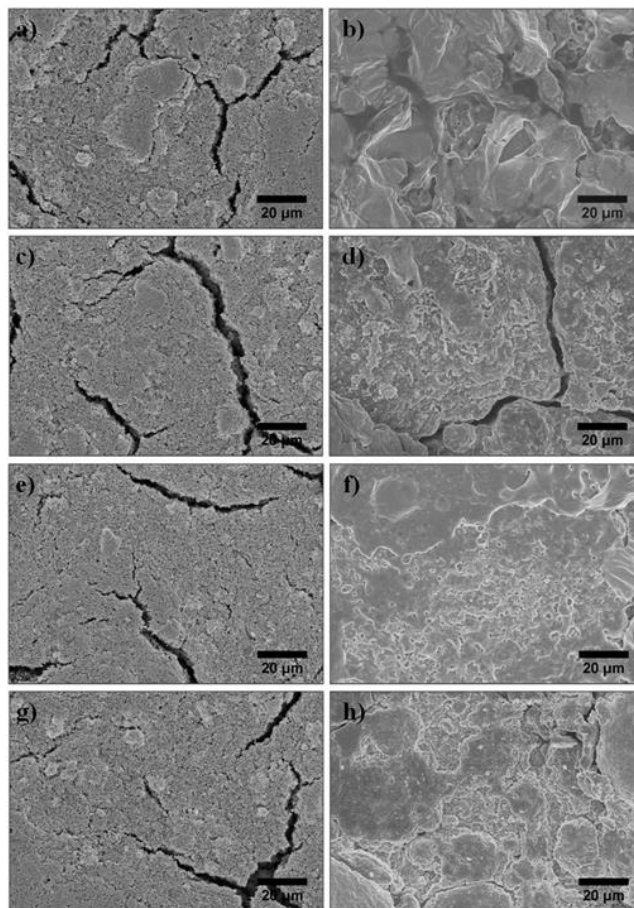


Fig. 7. Cyclic voltammetry profiles of the Si/Ag nanocomposite electrodes modified with different amounts of MPTMS (Si: 0.2 g, Ag: 0.1 g), M-0 (a, 0 g), M-0.2 (b, 0.2 g), M-0.6 (c, 0.6 g), and M-0.8 (d, 0.8 g).

It indicates that an activation process likely happens for the lithiation/delithiation. During the anodic process, two peaks at around 0.3 V and 0.5 V are ascribed to the de-lithiation process from amorphous  $\text{Li}_x\text{Si}$  to amorphous  $\text{Si}^{40, 42}$ . No extra peaks appear in the CV test. It implies that the silver nanoparticles only act as conductive agents and do not participate in the alloying process with lithium. As shown in Figure 7, the Si/Ag nanocomposites with different amounts of MPTMS exhibit very similar CV profiles, which suggest that the addition of MPTMS does not modify the fundamental lithiation/de-lithiation process of the Si nanoparticles.



*Fig. 8. SEM images of the Si/Ag nanocomposites modified with different amounts of MPTMS before (a, c, e, and g) and after (b, d, f, and h) 100 cycles: M-0 (a, b, 0 g), M-0.2 (c, d, 0.2 g), M-0.6 (e, f, 0.6 g), and M-0.8 (g, h, 0.8 g).*

Fig. 8 shows the morphology change of the electrodes before and after 100 cycles. It can be seen that the particulate feature of the electrodes is less visible after cycling, which may be due to the formation of the SEI layer on the electrode surface. Furthermore, the bare Si/Ag nanocomposite electrode is severely fractured after 100 cycles induced by mechanical stress due to volume change of silicon. Compared to the bare Si/Ag electrode, the Si/Ag nanocomposite electrodes modified with MPTMS are much more structurally integrated. It implies that the cross-linking of MPTMS between the silicon and silver nanoparticles helps to keep the structural integrity of the electrodes, leading to improved cyclic stability as shown by the electrochemical test.

#### 4. Conclusions

In summary, a new concept using (3-Mercaptopropyl) trimethoxyl silane (MPTMS) as cross-linking agent between silicon and silver nanoparticles has been successfully developed to

improve the electrochemical performance of the silicon nanoparticle electrode. The XRD experiment proves that the incorporation of the MPTMS does not modify the crystallinity of both the silicon and silver nanoparticles. The existence of MPTMS within the Si/Ag nanocomposite is confirmed by the FTIR measurement. The galvanostatic discharge/charge measurement indicates that the Si/Ag nanocomposites modified with different amounts of MPTMS show very similar discharge/charge profiles.

The addition of MPTMS significantly improves the cyclic performance of the Si/Ag nanocomposite. A reversible capacity of 517 mAh/g is achieved with the high electrode mass loading density of more than 1 mg/cm<sup>2</sup> after 100 cycles at 200 mA/g, compared to the almost zero capacity of the unmodified Si/Ag electrode. An outstanding rate performance is also observed with the modification of MPTMS, where 1078 mAh/g is reached at 1000 mA/g compared to the 759 mAh/g capacity of the bare Si/Ag electrode. The EIS measurement shows that the incorporation of MPTMS effectively reduces the total resistance of the nanocomposites, which is consistent with the rate performance result. The SEM images of the electrodes before and after cycling confirm that the Si/Ag electrode modified with MPTMS bears better structure stability than the bare Si/Ag electrode, which is supposed to be responsible for improved cyclic performance.

### Acknowledgement

This research is funded by the Natural Science Foundation of China (51103172), the Zhejiang Nonprofit Technology Applied Research Program (2013C33190), and the open project of the Beijing National Laboratory for Molecular Science (20140138), the CAS-EU S&T cooperation partner program (174433KYSB20150013), and Ningbo Key Laboratory of Polymer Materials.

### References

- [1] V. Aravindan, Y.-S. Lee, S. Madhavi, *Adv. Energy Mater.* **5**(13), n/a-n/a. (2015).
- [2] V. Etacheri, R., Marom, R. Elazari, G. Salitra, D. Aurbach, *Energy Environ. Sci.* **4**(9), 3243. (2011).
- [3] J. B. Goodenough, K. S. Park, *J. Am. Chem. Soc.* **135**(4), 1167 (2013).
- [4] H. Li, Z. Wang, L. Chen, X. Huang, *Adv. Mater.* **21**(45), 4593 (2009).
- [5] J. Niu, S. Zhang, Y. Niu, R. Song, H. Song, X. Chen, J. Zhou, S. Hong, *RSC Adv.* **4**(56), 29435 (2014).
- [6] S. H. Choi, D. S. Jung, J. W. Choi, Y. C. Kang, *Chem. - Eur. J.*, **21**(5), 2076 (2015).
- [7] T. Jaumann, M. Herklotz, M. Klose, K. Pinkert, S. Oswald, J. Eckert, L. Giebeler, *Chem. Mater.*, **27**(1), 37 (2015).
- [8] U. Kasavajjula, C. Wang, A. J., Appleby, *J. Power Sources.*, **163**(2), 1003 (2007).
- [9] B. Liang, Y. Liu, Y. Xu, *J. Power Sources.* **267**, 469 (2014).
- [10] D. Ma, Z. Cao, A. Hu, *SNano-Micro Lett.* **6**(4), 347 (2014).
- [11] M. T. McDowell, S. W. Lee, W. D. Nix, Y. Cui, *Adv. Mater.* **25**(36), 4966 (2013).
- [12] M. Osiak, H. Geaney, E. Armstrong, C. O'Dwyer, *J. Mater. Chem. A.* **2**(25), 9433 (2014).
- [13] P. Roy, S. K. Srivastava, *J. Mater. Chem. A* **3**(6), 2454 (2015).
- [14] C. Xu, F. Lindgren, B. Philippe, M. Gorgoi, F. Björefors, K. Edström, T. Gustafsson, *Chem. Mater.* **27**(7), 2591 (2015).
- [15] M. Ge, J. Rong, X. Fang, C. Zhou, *Nano Lett.* **12**(5), 2318 (2012).
- [16] N. Liu, Z. Lu, J. Zhao, M. T. McDowell, H. W. Lee, W. Zhao, Y. Cui, *Nat. Nanotechnol.* **9**(3), 187 (2014).
- [17] N. Liu, H. Wu, M. T. McDowell, Y. Yao, C. Wang, Y. Cui, *Nano Lett.* **12**(6), 3315 (2012).
- [18] X. R. Liu, X. Deng, R. R. Liu, H. J. Yan, Y. G. Guo, D. Wang, L. J. Wan, *Mater. Interfaces* **6**(22), 20317 (2014).

- [19] J. Ryu, S. Choi, T. Bok, S. Park, *Nanoscale* **7**(14), 6126 (2015)
- [20] Y. Yao, M. T. McDowell, I. Ryu, H. Wu, N. Liu, L. Hu, W. D. Nix, Y. Cui, *INano Lett.* **11**(7), 2949 (2011).
- [21] S. Fang, L. Shen, G. Xu, P. Nie, J. Wang, H. Dou, X. Zhang, *ACS Appl. Mater. Interfaces* **6**(9), 6497 (2014).
- [22] G. Grinbom, D. Duveau, G. Gershinsky, L. Monconduit, D. Zitoun, *Chem. Mater.* **27**(7), 2703 (2015).
- [23] Q. He, C. Xu, J. Luo, W. Wu, J. Shi, *Chem. Commun.* **50** (90), 13944 (2014).
- [24] H. Wang, H. Huang, L. Chen, C. Wang, B. Yan, Y. Yu, Y. Yang, G. Yang, *ACS Sustainable Chem. Eng.* **2**(10), 2310 (2014).
- [25] N. Wang, T. Hang, H. Ling, A. Hu, M. Li, *J. Mater. Chem. A* **3**(22), 11912 (2015).
- [26] P. Wu, H. Wang, Y. Tang, Y. Zhou, T. Lu, *ACS Appl. Mater. Interfaces* **6** (5), 3546 (2014).
- [27] Y. Xu, Y. Zhu, C. Wang, *J. Mater. Chem. A* **2**(25), 9751 (2014).
- [28] R. Yi, J. Zai, F. Dai, M. L. Gordin, D. Wang, *Nano Energy* **6**, 211 (2014).
- [29] Q. Hao, D. Zhao, H. Duan, Q. Zhou, C. Xu, *Nanoscale* **7** (12), 5320 (2015).
- [30] G. Talla, R. K. Guduru, B. Q. Li, P. S. Mohanty, *Solid State Ionics* **269**, 8 (2015),
- [31] X. Yang, Z. Wen, S. Huang, X. Zhu, X. Zhang, *Solid State Ionics* **177**(26-32), 2807 (2006).
- [32] S. Yoo, J.-I. Lee, S. Ko, S. Park, *Nano Energy* **2**(6), 1271 (2013).
- [33] Y. Yu, L. Gu, C. Zhu, S. Tsukimoto, P. A. van Aken, J. Maier, *Adv. Mater.* **22**(20), 2247 (2010).
- [34] W. Zhao, N. Du, C. Xiao, H. Wu, H. Zhang, D. Yang, *J. Mater. Chem. A* **2**(34), 13949 (2014).
- [35] B. Lee, S. Koo, *J. Ind. Eng. Chem.* **18**(3), 1191 (2012).
- [36] D. I. Tee, M. Mariatti, A. Azizan, C. H. See, K. F. Chong, *Compos. Sci. Technol.* **67**(11-12), 2584 (2007).
- [37] I. U. Vakarelski, C. E. McNamee, K. Higashitani, *Colloids Surf., A* **295** (1-3), 16 (2007).
- [38] M. Cai, M. Ho, J. E. Pemberton, *Langmuir* **16** (7), 3446 (2000).
- [39] Wade R. Thompson; Mei Cai, Mankit Ho, J. E. Pemberton, *Langmuir* **13**(8), 2291 (1999).
- [40] M. Gu, S. Ko, S. Yoo, E. Lee, S. H. Min, S. Park, B.-S. Kim, *J. Power Sources.* **300**, 351 (2015).
- [41] J. Wang, C. Wang, Y. Zhu, N. Wu, W. Tian, *Ionics* **21**(2), 579 (2014).
- [42] Y. Yang, D. Chen, B. Liu, J. Zhao, *BACS Appl. Mater. Interfaces* **7**(14), 7497 (2015).